J Braz. Soc. Mech. Sci. Eng. (2015) 37:1515–1528
DOI 10.1007/s40430-014-0294-0

TECHNICAL PAPER

Parameter design in friction welding of Al/SiC/Al_2O_3 composite using grey theory based principal component analysis (GT-PCA)

R. Adalarasan · A. Shanmuga Sundaram

Received: 20 June 2014 / Accepted: 2 December 2014 / Published online: 23 December 2014

Abstract Solid-state welding processes have widened the scope of joining metal matrix composites. The aim of this work was to study the possibility of producing good quality joints with Al/SiC/Al_2O_3 composites using continuous drive friction welding. Taguchi's L_9 orthogonal array was used to study the effect of welding parameters like frictional pressure, upset pressure, burn off length and rotational speed on the quality characteristics of joints. The quality of joints was evaluated by observing the tensile strength, elongation and micro hardness. An integrated approach of GT-PCA which combines the methodology of grey theory and principal component analysis (PCA) was used to predict the optimal level of friction welding parameters. Frictional pressure was identified as the prime parameter affecting the observed responses. Microstructure of the weld zone was examined using optical microscopy and the fractured surface was also investigated using the field emission scanning electron microscopy images.

Keywords Friction welding · Grey Taguchi · Principal component analysis · Optimization · Metal matrix composites

Technical Editor: Alexandre Mendes Abrao.

R. Adalarasan (✉)
Department of Mechanical Engineering, Saveetha Engineering College, Chennai 602105, India
e-mail: adalarasan@saveetha.ac.in; adalno1@yahoo.co.in

A. S. Sundaram
Department of Mechanical Engineering, Sree Sastha Institute of Engineering and Technology, Chennai 602123, India

1 Introduction

The aluminium-based metal matrix composites (MMCs) were known for their better mechanical properties and those with ceramic reinforcements exhibit an isotropic mechanical behaviour offering the advantage of being processed by conventional secondary routes [1]. The role of welding was important in component manufacturing and increased industrial applications of these MMCs create an urge to explore their welding characteristics. However, one of the main limitations in the use of these materials was concerns about their joining. Unnecessary microstructural changes including grain boundary corrosion and wider heat affected zone (HAZ) were observed during fusion welding of MMCs and the ceramic reinforcement phase was found to produce an undesired matrix-reinforcement reaction [2]. Further the melting zone was found to be wider during welding of Al99-SiC composites [3]. A solid-state joining process like friction welding (FW) could offer a possible solution as the temperature involved was restricted below the melting point of parent material. FW had gained importance in fabrication industries because of its merits including a shorter production time, lesser HAZ and lower energy input. The joint coalescence was produced by rotating one component and keeping it in contact with a static component to generate frictional heat at the interface. An axial pressure applied during the process warrants an intimate contact between the parts restricting the deformation to the volume of material close to original interface.

Dissimilar friction welded joints were found to possess good strength with reasonable ductility and the fractured surface exhibited signs of ductile mode of failure [4]. Upset pressure was identified as a prominent factor affecting the quality characteristics of joints. However, the formation of intermetallic compounds at the interface of these joints

was found to degrade its strength [5, 6]. The frictional pressure, spindle speed and burn off length were identified as the significant factors affecting the quality characteristics of joints involving aluminium alloy AA7075-T6 and the hardness in the heat-affected zone (HAZ) was found to be lesser than that in the weld zone [7]. Friction welded stainless steel joints were found to possess good mechanical and microstructural characteristics with fine grains at the joint interface but metal loss was observed to increase with the friction time [8]. Grain refinement was also observed in the weld region which was attributed to the thermal and mechanical stresses at the interface of joints [9]. Heat treatment was essential in case of dissimilar joints exhibiting hardening in the weld region [10].

From the existing literature, it was understood that the quality of friction welded joint was affected by the process parameters like frictional pressure, upset pressure, burn off length and speed. Identifying the optimal parameter setting was vital to obtain the desired quality characteristics. Methods employed to solve multi response optimization problems include the grey relational analysis (GRA), response surface methodology (RSM), principal component analysis (PCA), artificial neural network (ANN), genetic algorithm (GA) and regression analysis [11]. A comparison of the performance status of various methods had revealed the superiority of grey based theory in giving better results [12]. Generally, grey relational grade was used as the quality index in GRA and variance analysis was also performed to identify the impact of various parameters on quality characteristics [13]. GRA was used to find the optimal friction stir welding parameters and their contribution could be identified using analysis of variance (ANOVA) and Taguchi concepts [14]. An adequate mathematical model of second order generated using RSM could be used in predicting and optimizing the responses as well [15]. However, RSM was observed to lose its power in irregular regions. A survey of optimization methods reveal a high degree of interest in employing ANN but the disadvantage lies in its greater computational burden and difficulty in training the network. Taguchi's statistical approach was used for optimization of process parameters in different areas of manufacturing and the technique was supplemented by ANOVA [16–18], but these techniques were observed to converge in local optima. The combined approach of ANN and real coded genetic algorithm (RCGA) was also found to be effective in eliminating the difficulties associated with training ANN [19, 20].

Principal component analysis is an exploratory data analysis and simplest among the Eigenvalue-based multivariate analyses. It was superior to analysis based on Fourier transforms and better than factor analysis in accounting for the variance. Datta et al. [21] proved the application feasibility of PCA in optimizing multi responses in arc welding and showed satisfactory results. Multi response optimization could be performed using either PCA in genuine format or as a hybrid with other techniques to find optimality criteria in various manufacturing processes [22, 23]. Multi objective desirability approach was also observed to predict the optimal operating condition using a model developed through RSM [24]. Combined neuro-fuzzy systems were found to be effective in modelling and optimization in various mechanical processes [25, 26]. The first report on linear friction welding of Al/SiCp composites proved that it was an attractive welding technology for particulate reinforced composites. The joints were observed to be of good quality but were found to fail in the thermo mechanically affected zone during external loading [27]. While joining AA2124/SiC/25p–T4 composite plates by friction stir welding it was observed that the tensile strength of butt joints formed was lower than that of parent material [28].

A decent amount of literature was available on friction welding of similar and dissimilar materials but research work in the area of friction welding of Al/SiC/Al_2O_3 composites was scarce. Further within the scientific literature, little computational attention was given to parameter design in friction welding of MMCs. Hence in this study Al/SiC/Al_2O_3 composites were joined by solid-state FW process using structured experimental design. The joints were mechanically assessed and the optimal parameter setting was identified using an integrated approach of grey theory based principal component analysis (GT-PCA). The results were validated using confirmation experiment.

2 Multi response optimization using grey theory based principal component analysis

The multi response optimization was viewed as an effective off-line quality control approach to improve the product quality. Optimization of multiple responses in the process of friction welding was more complex than single response optimization. The concept of grey coefficient was used in PCA to form an integrated approach (GT-PCA) for predicting the optimal setting of parameters. Taguchi techniques use signal-to-noise (S/N) ratio instead of standard deviation to compare the responses. The methodology of GT-PCA approach was discussed in Sects. 2.1 and 2.2.

2.1 Phase I: grey relational analysis

Step 1: Perform data pre-processing and normalization to reduce the effect of using various units and scaling the data for further analysis [30]. A quality characteristic (response) was one which governs the outcome of a process. The S/N ratio (η_{ij}) was taken as a measure of quality [13]. It was calculated for the *larger-the-better* type using Eq. 1.

$$\text{S/N Ratio}\left(\eta_{ij}\right) = -10\log_{10}\left(\frac{1}{r}\right)\sum_{k=1}^{r}\frac{1}{\left(y_{ij}\right)_k^2}, \tag{1}$$

where y_{ij} is the observed response value, $i = 1,2,3\ldots n$, $j = 1,2,\ldots m$, n is the number of responses, m is the number of trials and r is the number of replications.

Step 2: Calculate the normalised S/N ratio (Z_{ij}) using Eq. 2 to avoid the effect of variability among the S/N ratio [30] and compute grey relational coefficient [GRC(γ)] using Eq. 3 to express the relationship between the ideal and the actual normalised experimental results from the normalised S/N ratio [23].

$$Z_{ij} = \frac{y_{ij} - \min(y_{ij}, i = 1,2,\ldots,m)}{\max(y_{ij}, i = 1,2,\ldots,m) - \min(y_{ij}, i = 1,2,\ldots,m)} \tag{2}$$

$$\gamma_i^j = \frac{\Delta\min + \xi\Delta\max}{\Delta_{oj}(i) + \xi\Delta\max} \tag{3}$$

$\Delta_{oj} = \left\|z_o(i) - z_j(i)\right\|$ is the absolute value of the difference between $z_o(i)$and$z_j(i)$, $z_o(i)$is the reference sequence ($z_o(i)$=1; i=1,2,…,n), $z_j(i)$is the specific comparison sequence, $\Delta\min = \min_{\forall j\in i}\min_{\forall i}\left\|z_o(i) - z_j(i)\right\|$ is the smallest value of $z_j(i)$ and $\Delta\max = \max_{\forall j\in i}\max_{\forall i}\left\|z_o(i) - z_j(i)\right\|$ is the largest value of $z_j(i)$.

ξ is the distinguishing coefficient whose value was taken as 0.25 to ensure unbiased analysis of the responses.

2.2 Phase II: principal component analysis

The PCA approach uses orthogonal transformation to convert a set of observed variables (correlated variables) into a set of principal components (uncorrelated components) which are generally not independent components and hence do not require separate independent components analysis [21, 23].

Step 3: Use the GRC values (obtained from the grey Taguchi theory) to form the multiple quality characteristic array in PCA. Develop the correlation coefficient matrix (R) using the multiple quality characteristic array. Compute the Eigenvalues and Eigenvectors using Eq. 4 [23]. Also calculate the proportion of explained variation (δ_k) of the individual components using Eq. 5.

$$(R - \lambda_k I_m)\ V_{ik} = 0 \tag{4}$$

$$\delta_k = \frac{\lambda_k}{\sum_{k=1}^{n}\lambda_k}, \tag{5}$$

where λ_k is the Eigenvalue and $\sum_{k=1}^{n}\lambda_k = n$, $k = 1, 2, \ldots, n$; $V_{ik} = [a_{k1}\ a_{k2}\ \ldots a_{kn}]^T$ is the Eigenvector corresponding to Eigenvalue λ_k.

Step 4: Find the principal components (Z_{mk}) using Eq. 6 and determine the weighted sum of principal components identified as multi attribute performance index (MAPI) using Eq. 7 for each trial [21]. MAPI was taken as the measure of performance in GT-PCA approach.

$$Z_{mk} = \sum_{i=1}^{n} x_m(i)\cdot V_{ik}, \tag{6}$$

where Z_{m1} is the first principal component, Z_{m2} is the second principal component and so on. $x_m(i)$ indicate the values in multiple quality characteristic array.

$$\text{MAPI}_m = \sum_{k=1}^{n}(\delta_k \times Z_{mk}) \tag{7}$$

Step 5: Identify the optimal level of parameters based on MAPI values and calculate the main effect (ε_i) of the parameters for each level using Eq. 8.

$$\varepsilon_i = \max\left(\text{MAPI}_{ij}\right) - \min\left(\text{MAPI}_{ij}\right) \tag{8}$$

The best level j^* of the controllable factor 'i' is selected as $j^* = \max\ (\text{MAPI}_{ij})$

Step 6: Compute the predicted S/N ratio ($\overline{\eta}$) at the selected optimal level of parameters using Eq. 9 [30].

$$\overline{\eta} = \eta_m + \sum_{i=1}^{f}(\overline{\eta_i} - \eta_m) \tag{9}$$

where η_m is the average S/N ratio, f is the number of control factors and $\overline{\eta}_i$ is the average S/N ratio corresponding to the ith factor on the jth level.

Step 7: Perform the analysis of variance (ANOVA) on the MAPI values to supplement GT-PCA technique.

Step 8: Conduct confirmation test for validation.

3 Experimental design and observation

3.1 Materials

The matrix material used in the study was Al6061 alloy which finds wide applications in the field of aerospace and automobile engineering. It was reinforced with the fine particles of Silicon carbide (SiC) and alumina (Al_2O_3) in weight fractions of 10 % each to form Al/SiC/Al_2O_3 composite. In-situ fabrication was done by dispersing the reinforcing particles in liquid Al6061 alloy. Stir casting setup (Fig. 1a) was used to produce the MMC rods each of length 80 mm and diameter 18 mm as shown in Fig. 1b. The rods were subjected to inspection by X-ray radiography to confirm the absence of defects and the selected rods were finally machined in a lathe to bring down the diameter and length to 16 mm and 75 mm, respectively.

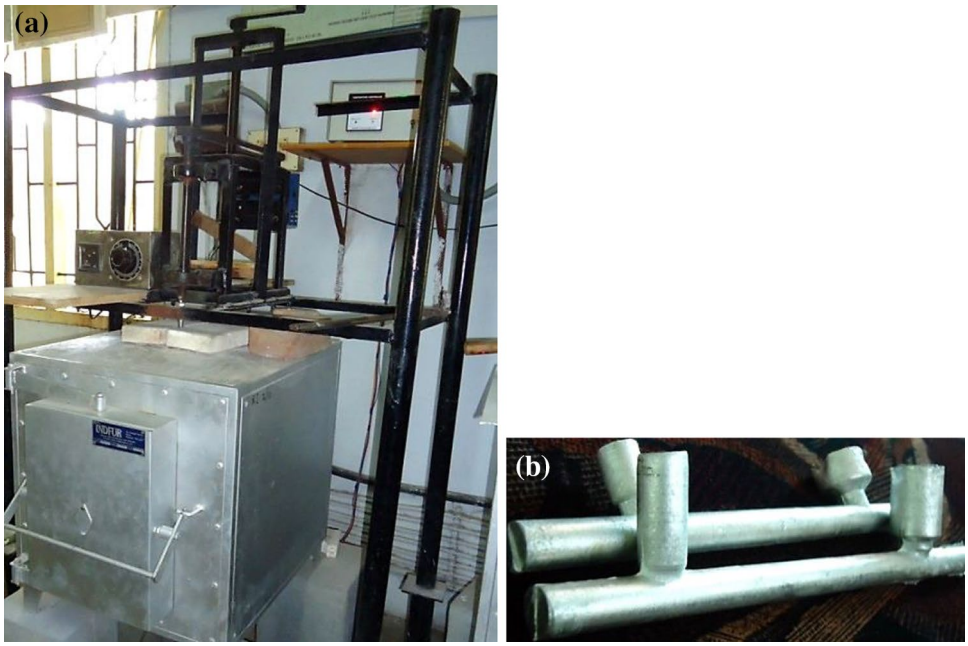

Fig. 1 **a** Stir casting setup, **b** cast Al/SiC/Al_2O_3 rods

3.2 Continuous drive friction welding

In continuous drive friction welding process, one part was held in a chuck (connected to a motor drive) and rotated at a constant rpm while the other part to be joined was kept stationary in a motion system capable of imparting an axial force. The work pieces were brought together under pressure and the frictional heat generated at the interface due to rubbing action forms the joint. A friction welding machine (Fig. 2a) of 20 T capacity, manufactured by ETA technology, was employed to form the joints. An AC servo motor rated at 20 HP was used to drive the spindle at a maximum speed of 2,800 rpm. A load cell controlled by a hydraulic servo valve was used to read the frictional and upset pressure directly. The FW machine setup precisely controlled by a PLA based system was designed to achieve transition from friction to forging stage automatically. One of the parent rods to be joined was held in the chuck as shown in Fig. 2b and was rotated at constant rpm while the other was kept stationary as shown in Fig. 2c in a system capable of producing axial motion.

3.3 Experimentation

The four dominant welding parameters chosen for the study were frictional pressure, upset pressure, burn off length and rotational speed [5–9]. The frictional pressure influences the heat input and rotational speed determines the interface temperature [5]. The decrease in length of the specimen due to formation of flash is termed as burn off. The upset pressure and burn off length control the solid-state deformation at the interface of joining parts. The next step was concerned with the selection of range of input parameters that would be safe for setting parameters at levels where welding trials would not end in a failure.

It was understood that picking a parameter either too high or low in value would degrade the quality of bonds. Pilot welding trials were conducted for sorting out the acceptable upper and lower bounds of parameters for which joints were formed without any visible defects or failure. Further, it was observed that a frictional pressure of 60 MPa produced strong joints and a still lower level was desired for finer grains in joints involving aluminium [6, 8]. However, a higher value of upset pressure (120 MPa) was observed to produce good joints with softer materials like copper and aluminium [8]. Rotational speed of 2,000 rpm combined with a larger burn off length was observed to form good quality joints [7]. Hence three levels were considered for each of the four welding parameters based on literature [6–8] and Taguchi's L_9 orthogonal array was used to conduct the welding trials. The chosen levels of various parameters are presented in Table 1.

The welding trials were performed in random order to shrink the effects of extraneous factors [11]. Two replicates were formed for each combination of process parameters during which equal overhung lengths were ensured on both the stationary and rotating parts. The actual photograph of the joints is shown in Fig. 3. The responses studied were the tensile strength (TS) in N/mm^2, percentage elongation (E) and micro hardness in the weld zone (H-WZ) and at heat-affected zone (H-HAZ). Micro hardness was found out using a Vickers hardness tester by applying a load of 0.5 kg for 20 s and the actual measurements were taken

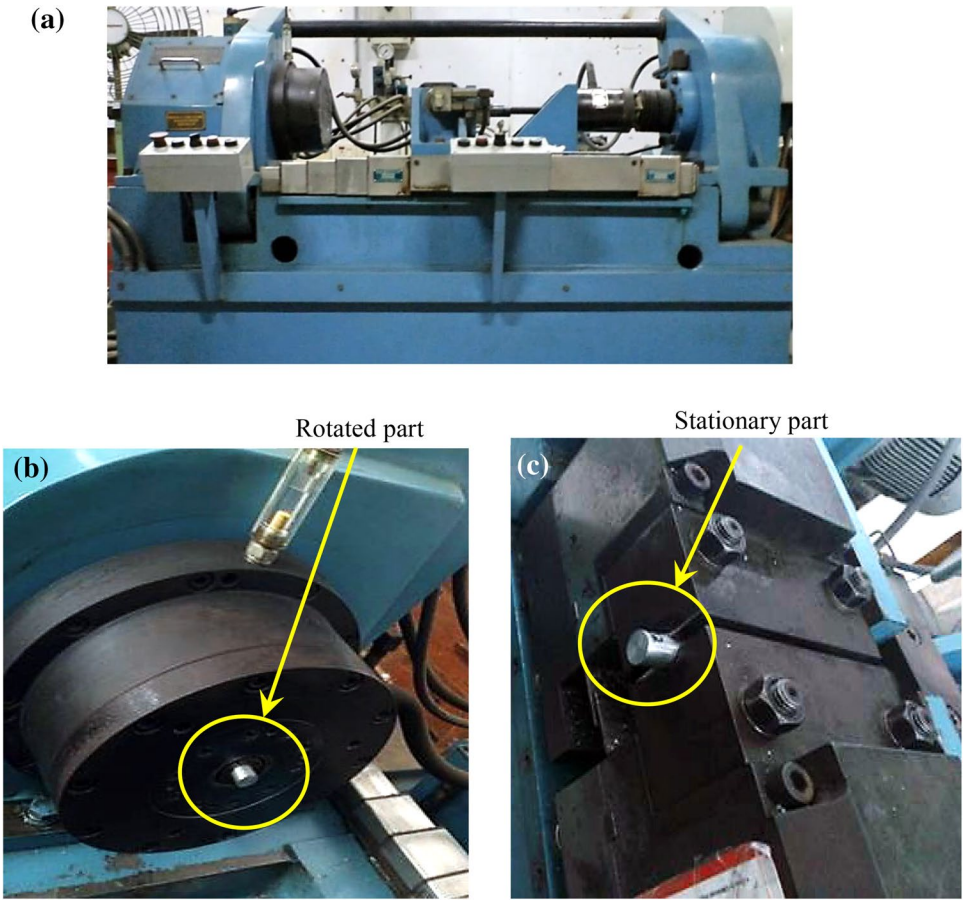

Fig. 2 Friction welding set up, **a** friction welding machine, **b** part rotated in the chuck, **c** stationary part in axial loading system

Table 1 Input parameters and their levels

Parameters	Notation	Unit	Levels of parameters		
			Level 1	Level 2	Level 3
Frictional pressure	A	MPa	40	50	60
Upset pressure	B	MPa	100	120	145
Burn off length	C	mm	1	2	3
Rotational speed	D	rpm	2,000	2,250	2,500

from samples sectioned in the transverse direction at the weld zone and at the HAZ. The friction welded solid-state bonds were characterized by the presence of reduced HAZ compared to fusion welding which involves melting of parent material. The HAZ was observed to spread to a maximum distance of 2 mm on both sides of the bond line [27]. The Tension test was carried out in computerized tensile testing machine after preparing the specimen according to ASTM B557 standard during which all the samples were observed to fail either in the weld zone or close to the bond line. The photograph of fractured samples is shown in Fig. 4. The responses observed for the different combinations of input parameters designed by L_9 orthogonal array is shown in Table 2.

3.4 Implementation of GT-PCA methodology

Optimization of multiple quality characteristics in friction welding was challenging than optimization of a single response. The grey Taguchi theory was used in PCA to form quality measure of MAPI to represent the four responses. The data were pre-processed by calculating the values of S/N ratio for scaling the data and normalised S/N ratio was found out to avoid the effect of variability among the S/N ratio. The GRC values were also calculated to express the link between the ideal and the actual normalised experimental results. The normalised values along with the GRC are listed in Table 3.

The multiple quality characteristic array was formed using the GRC values. The Eigenvalues and the proportion of explained variation (PEV) were calculated from the correlation coefficient array and listed in Table 4. PEV was a friendly measure to explain the reliability of approach and was used to investigate the effects of various levels of parameters.

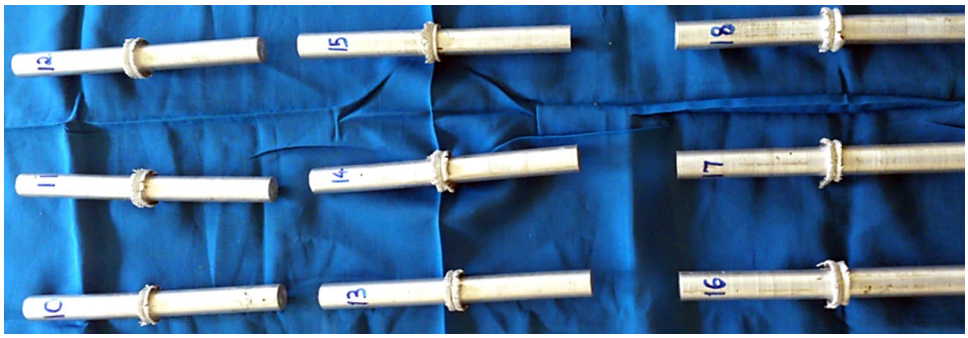

Fig. 3 Photograph of friction welded joints

Fig. 4 Fractured sample during tensile testing: sample 4 (frictional pressure 50 MPa, upset pressure 100 MPa, burn off length 2 mm and speed 2,500 rpm) and sample 5 (frictional pressure 50 MPa, upset pressure 120 MPa, burn off length 3 mm and speed 2,000 rpm)

The principal components (Z_{mk}) were calculated using Eq. 6 and the weighted sum of principal components (MAPI) was calculated using Eq. 7 for each trial. MAPI was taken as the measure of performance and it was used as a single representative of all the four responses. The first principal component represents the direction in search space along which the largest variance was observed. Orthogonally to the first, second principal component direction was the one which maximizes the variances in all the directions perpendicular to the first component. The principal components and calculated MAPI values for each trial are listed in Table 5.

Table 2 Combination of welding parameters for various trial and the observed responses

Run	Process parameters				Experimental results (responses)			
	A	B	C	D	TS	E	H-HAZ	H-WZ
1	40	100	1	2,000	115.87	2.02	62.8	65.8
2	40	120	2	2,250	91.23	2.00	69.4	72.4
3	40	145	3	2,500	90.75	2.00	62.5	67.4
4	50	100	2	2,500	101.49	1.60	62.0	67.5
5	50	120	3	2,000	70.79	4.74	70.2	71.4
6	50	145	1	2,250	115.62	6.00	70.6	72.0
7	60	100	3	2,250	76.78	5.60	69.8	73.3
8	60	120	1	2,500	58.39	5.50	71.8	72.6
9	60	145	2	2,000	99.41	4.84	71.1	72.2

Table 3 S/N ratio, normalised S/N ratio and GRC values

Trial	S/N ratio				Normalised Normalised S/N ratio				GRC			
	TS	E	H-HAZ	H-WZ	TS	E	H-HAZ	H-WZ	TS	E	H-HAZ	H-WZ
1	41.279	6.107	35.959	36.365	1.000	0.176	0.087	0.000	1.000	0.233	0.215	0.200
2	39.203	6.021	36.827	37.195	0.651	0.169	0.768	0.886	0.417	0.231	0.519	0.686
3	39.157	6.021	35.918	36.573	0.643	0.169	0.055	0.223	0.412	0.231	0.209	0.243
4	40.128	4.082	35.848	36.586	0.807	0.000	0.000	0.236	0.564	0.200	0.200	0.247
5	36.999	13.51	36.927	37.074	0.281	0.822	0.846	0.757	0.258	0.584	0.619	0.507
6	41.261	15.56	36.976	37.147	0.997	1.000	0.885	0.834	0.988	1.000	0.685	0.601
7	37.705	14.96	36.877	37.302	0.400	0.948	0.807	1.000	0.294	0.827	0.565	1.000
8	35.327	14.80	37.122	37.219	0.000	0.934	1.000	0.911	0.200	0.792	1.000	0.738
9	39.949	13.69	37.037	37.171	0.776	0.837	0.933	0.860	0.528	0.606	0.789	0.641

The plot of MAPI values for the various trials is shown in Fig. 5. Higher value of MAPI was desired irrespective of the nature of quality characteristics. The parameter combination corresponding to the trial number eight was observed to possess the peak value of MAPI (1.0032). Hence the operating condition corresponding to that trial would produce better responses.

The effects of parameter levels on MAPI are shown graphically in Fig. 6. The variations of MAPI for various trials indicate the significance of chosen levels of different parameters. The levels of parameters for which MAPI values are higher would give better responses.

The optimal level of parameters was identified based on MAPI. The main effect (ε_i) of the parameters for each level is presented in Table 6. The best level j^* of a parameter 'i' was selected as $j^* = \max(\text{MAPI}_{ij})$.

Analysis of variance (ANOVA) was performed to supplement the GT-PCA technique. It was performed on the MAPI values which were taken as the overall representative of all the four responses. ANOVA was performed to predict the significant factors and their contribution in affecting the desired responses at a level of significance (α) of 0.05. The results of pooled ANOVA are presented in Table 7. The contribution of frictional pressure was found to be larger than that of remaining welding parameters (59.98 %). The main effects of the parameters on MAPI was studied to find the optimal level of welding parameters as $A_3B_2C_1D_2$ (Table 6) but a confirmation test becomes essential to validate the same.

Table 4 Eigenvalue and Eigenvector

Principal component	Eigenvalue (λ)	PEV (%)	Eigenvector
First	2.331	0.6555	[−0.300, 0.522, 0.566, 0.564]
Second	0.858	0.2413	[0.876, 0.446, 0.101, −0.066]
Third	0.133	0.0374	[−0.355, 0.714, −0.470, −0.379]
Fourth	0.234	0.0658	[0.125, 0.010, −0.067, 0.731]

Table 5 The principal components and MAPI values for the various trials

Trial	Principal components				MAPI
	Z_{m1}	Z_{m2}	Z_{m3}	Z_{m4}	
1	0.0561	0.9930	−0.3656	0.1315	0.2713
2	0.6761	0.4806	−0.4870	0.2090	0.5547
3	0.2527	0.4739	−0.1717	0.0924	0.2796
4	0.1875	0.5911	−0.2449	0.1199	0.2643
5	0.8637	0.5271	−0.1581	−0.0060	0.6870
6	0.9527	1.3606	−0.1865	0.1159	0.9534
7	1.2274	0.6341	−0.1582	0.3981	0.9779
8	1.3353	0.5964	−0.2554	−0.0974	1.0032
9	0.9661	0.7823	−0.3686	0.0128	0.8091

3.5 Confidence interval

The expected mean value of MAPI for the optimal setting (μ_{exp}) must be calculated to predict the optimal welding condition [31]. This was performed by employing Eq. 10.

$$\mu_{exp} = \overline{A}_3 + \overline{B}_2 + \overline{C}_1 + \overline{D}_2 - 3 \times \mu_{MAPI}, \quad (10)$$

where $\overline{A}_3$, $\overline{B}_2$, $\overline{C}_1$ and $\overline{D}_2$ were the mean values of the MAPI with the welding parameters at optimum levels and μ_{MAPI} was the overall mean of MAPI.

The expected mean of MAPI (μ_{exp}) for the optimal welding condition was calculated to be 1.316 and it was observed to be greater than that observed with the initial condition (1.0032). Confidence interval (CI) was calculated using Eq. 11 [31].

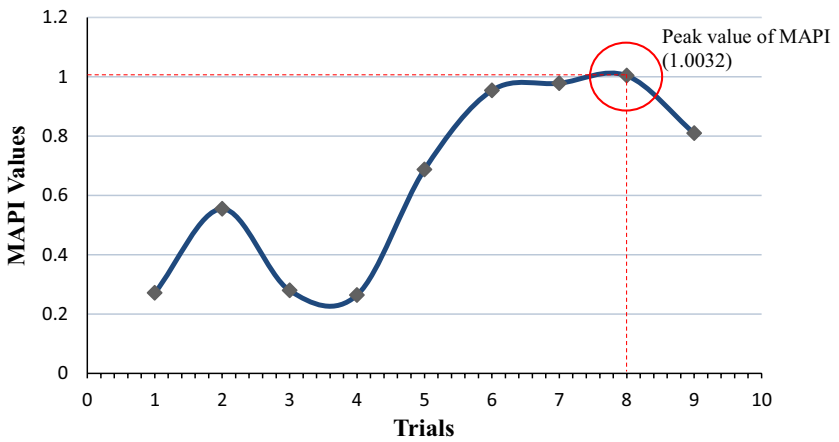

Fig. 5 Variation of MAPI values for various trials

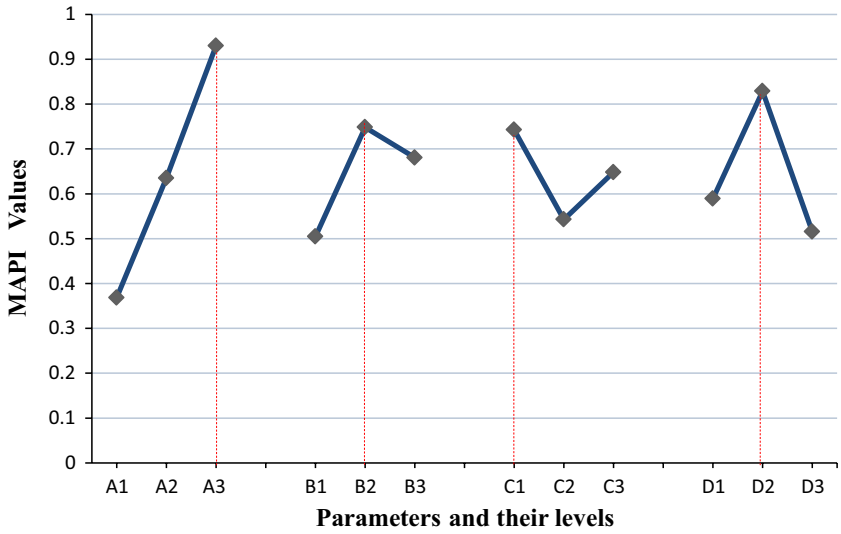

Fig. 6 Effect of parameter levels on MAPI

Table 6 The main effect of the parameters on MAPI

Parameters	Level 1	Level 2	Level 3	Max–min
A	0.3685	0.6349	**0.9301**	0.5615
B	0.5045	**0.7483**	0.6807	0.2438
C	**0.7427**	0.5427	0.6482	0.2000
D	0.5892	**0.8287**	0.5157	0.3130

Bold values correspond to the optimal level of studied parameters

$$\mathrm{CI} = \sqrt{F_\alpha(1, f_e) V_e \left[\frac{1}{n_{\mathrm{eff}}} + \frac{1}{R}\right]} = \pm 0.8424, \tag{11}$$

where $F_\alpha(1, f_e)$ is the F ratio at a level of significance ($\alpha = 0.05$), f_e indicates the error degrees of freedom, V_e is the error mean square, n_{eff} is the effective total number of tests and R is the number of replications in confirmation test.

$$(\mu_{\mathrm{exp}} - 0.8424) \leq \mu_{\mathrm{confirmed}} \leq (\mu_{\mathrm{exp}} + 0.8424)$$

$$0.4736 \leq \mu_{\mathrm{confirmed}} \leq 2.1584$$

The MAPI value at the optimal setting in the confirmation test ($\mu_{\mathrm{confirmed}}$) was found to be 1.4214. This value was observed to fall within the limits of 95 % CI of the predicted optimal condition. Further, the MAPI value of confirmation experiment was improved by 7.42 % from the predicted mean value.

4 Results and discussion

4.1 Effect of welding parameters on quality characteristics

All the welding parameters studied were found to influence the quality characteristics observed in the process. The rotational speed and frictional pressure were sustained for some time to warrant satisfactory thermal and mechanical conditioning at the interface. As the rotation was stopped, upset pressure was increased to maintain intimate contact between the parts resulting in plastic deformation near the bond interface. Taguchi techniques use S/N ratio (ratio of useful data to irrelevant information) for comparing the responses [11]. After calculating the S/N ratio corresponding to each experimental trial, the effect of a parameter at a particular level was computed by taking the average of all S/N ratios at the same level. The parameter level corresponding to maximum average S/N ratio was the desirable level, irrespective of the nature of quality characteristics observed. A graphical representation of the effect of different parameters at various levels is shown in Fig. 7.

Table 7 Results of the pooled ANOVA on MAPI

Source	SS	DOF	MS	F	P value	Contribution
SS_A	0.4734	2	0.2367	7.8872	0.1125	59.98
SS_B	0.0951	2	0.0475	1.5837	0.3870	12.05
SS_D	0.1607	2	0.0804	2.6777	0.2719	20.36
SS_{error}	0.0600	2	0.0300			7.607
SS_T	0.7892	8				100

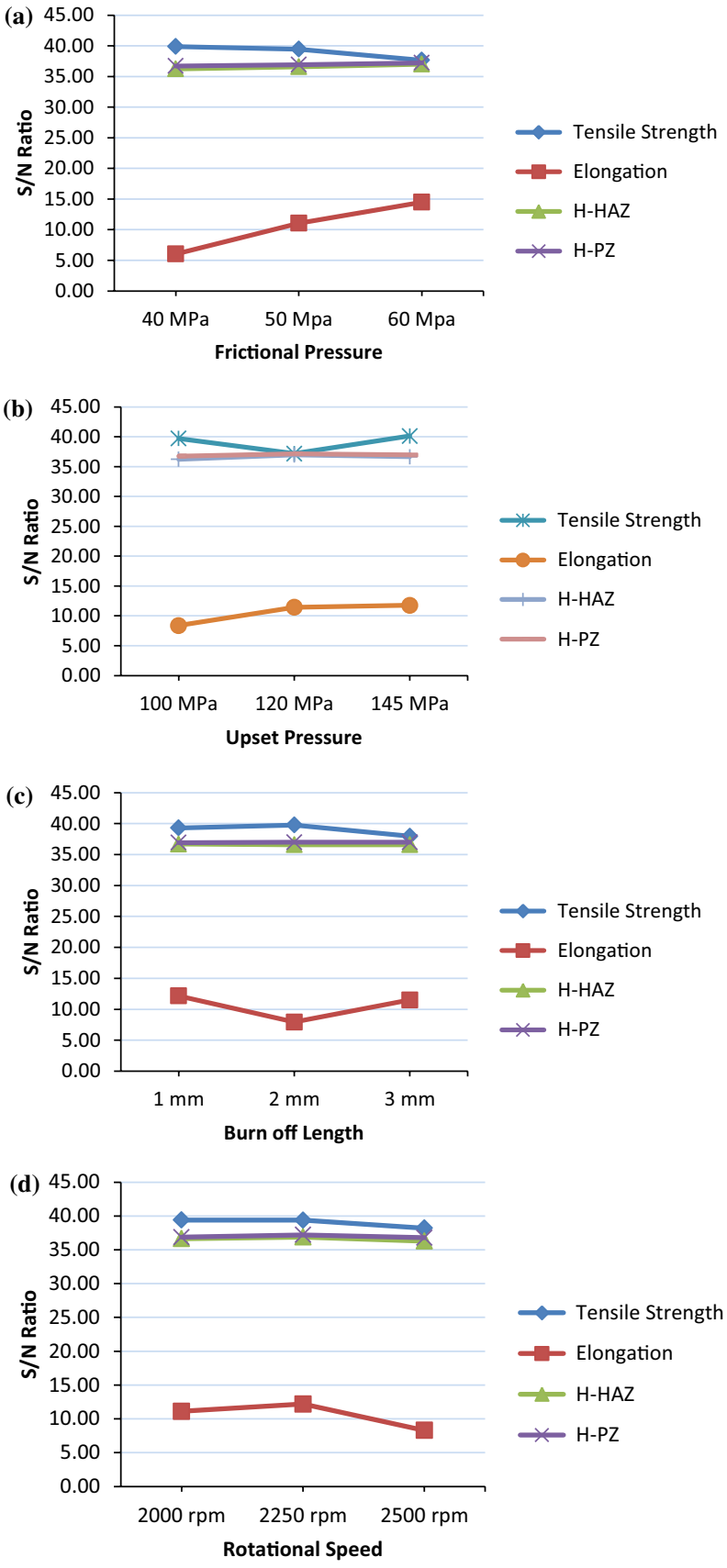

Fig. 7 Effect of friction welding parameters, **a** frictional pressure, **b** upset pressure, **c** burn off length, **d** rotational speed

Table 8 Comparison of the responses for the initial and optimal parameter setting

Responses	Initial parameter setting		GT-PCA parameter setting		Improvement	
	Observed S/N ratio	Response value	Predicted S/N ratio	Response value	Response value	%
TS	35.3268	58.39	36.5122	68.97	10.58	18.12
E	14.8073	5.5	18.6863	7.42	1.9	34.55
H-HAZ	37.1225	71.8	37.7201	75.2	3.4	4.74
H-WZ	37.2187	72.6	37.6406	77.1	4.5	6.20
Parameter setting	A_3 B_2 C_1 D_3		**A_3 B_2 C_1 D_2**			

Bold refers to the optimal setting of parameters sorted using GT-PCA approach

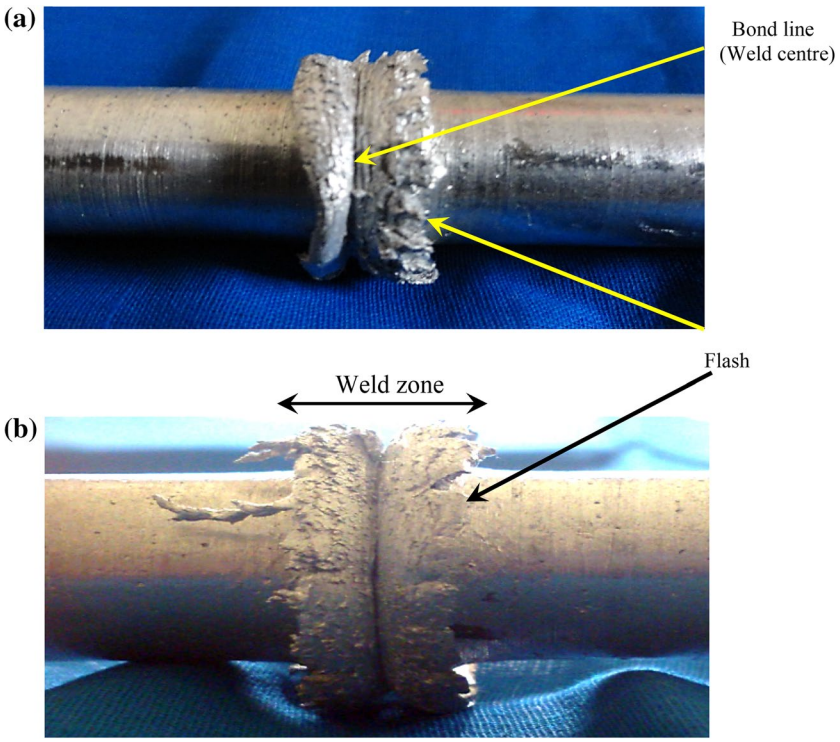

Fig. 8 Macroscopic view of the joint formed with **a** initial setting: (frictional pressure = 60 Mpa, upset pressure = 120 MPa, burn off length = 1 mm and speed = 2,500 rpm). **b** Optimal setting: (frictional pressure = 60 Mpa, upset pressure = 120 MPa, burn off length = 1 mm and speed = 2,250 rpm)

Frictional pressure ensures complete wearing out of surface asperities as one part was rotated in contact with the other. It was seen that a frictional pressure of 40 MPa was found to improve the tensile strength of joint (Fig. 7a) while the elongation was observed to be better at higher values of frictional pressure. Generally, an increase in frictional pressure was observed to improve the ductility of joints and less significant changes in hardness was noted with variation in levels of frictional pressure. An upset pressure of 145 MPa was found to enhance elongation (Fig. 7b) and hence the ductile property, but there was no significant change in micro hardness values with various levels of upset pressure. Hence a higher value of upset pressure (145 MPa) was desired to improve the quality characteristics of the joints as the tensile strength observed was also slightly higher than that obtained with the first level of upset pressure. Upset pressure was significant in inducing plastic deformation at the interface pushing the material around the circumference in the form of flash as bonding takes place.

It was observed that a burn off length of 2 mm produces joints with improved tensile strength relative to the first level of burn off length after which the strength starts to decrease; however, the elongation was observed to be good at a burn off length of 1 mm (Fig. 7c). The effect of burn off length on hardness was observed to be less significant. From Fig. 7d, it is seen that a lower value of speed (2,000 rpm) could produce joints with improved tensile strength while at higher level the strength was found to decrease slightly. However, for good elongation (ductility) of joint a moderate rotational speed (2,250 rpm) was desired. Generally, rotational speed along with frictional pressure was observed to play an important role in deciding the energy input at the interface and hence thermal softening. The micro hardness value was found to be higher in the plastic zone than at HAZ for all the joints produced. This

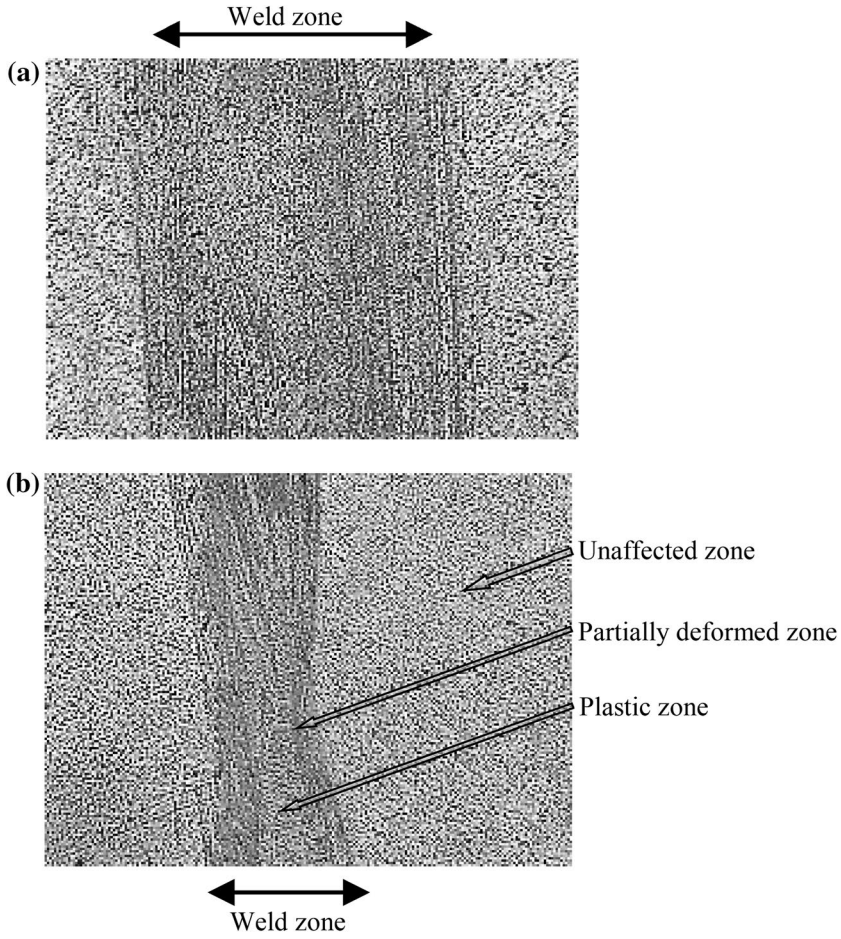

Fig. 9 Optical micrograph showing the weld zone in case of joints obtained with **a** initial parameters setting: (frictional pressure = 60 MPa, upset pressure = 120 MPa, burn off length = 1 mm and speed = 2,500 rpm). **b** Optimal parameters setting: (frictional pressure = 60 MPa, upset pressure = 120 MPa, burn off length = 1 mm and speed = 2,250 rpm)

was due to severe plastic deformation and localized strain hardening in the plastic zone.

4.2 Confirmation experiment

The confirmation experiment was performed to validate the optimal process parameter setting predicted by the GT-PCA algorithm. The responses obtained from the confirmation experiment conducted at the optimal parameter level (frictional pressure 60 MPa, upset pressure 120 MPa, burn off length 1 mm and speed 2,250 rpm) were compared with those obtained from the initial parameter setting (frictional pressure 60 MPa, upset pressure 120 MPa, burn off length 1 mm and speed 2,500 rpm). The combination of parameters for trial number eight (peak value of MAPI) was same as that of the initial setting. The result of confirmatory test is shown in Table 8. Subsequently the confirmatory test produced satisfactory results and an improvement in responses was observed.

4.3 Macroscopic analysis

The joints formed with the initial setting of parameters $A_3B_2C_1D_3$ (Fig. 8a) and the optimal parameters setting predicted by GT-PCA approach (Fig. 8b) were subjected to macroscopic visual analysis. The macroscopic image of the joint formed with initial setting of parameters and the optimal parameter setting is shown in Fig. 8. It was clearly observed that the flash was more uniform for the joint formed with optimal setting of parameters and that the width of flash was also uniform on both sides of the bond line (Fig. 8b). The curl of the flash was observed to be more symmetric and weld penetration was found to be better for the joint formed with optimal parameter setting (Fig. 8b). However, the ductile flow of material in the form of flash was clearly apparent in both the cases (Fig. 8a, b). The material expelled along the circumference at the weld interface was observed to be of same radial width which was an essential feature of good quality joint [27]. This could be clearly visualized in the case of optimal joint shown in Fig. 8b.

4.4 Microstructure characteristics at the weld zone

The integrity of the joints was analysed through the micrographs at the weld zone. The microstructural examination of joint (Fig. 9) indicates the absence of porous

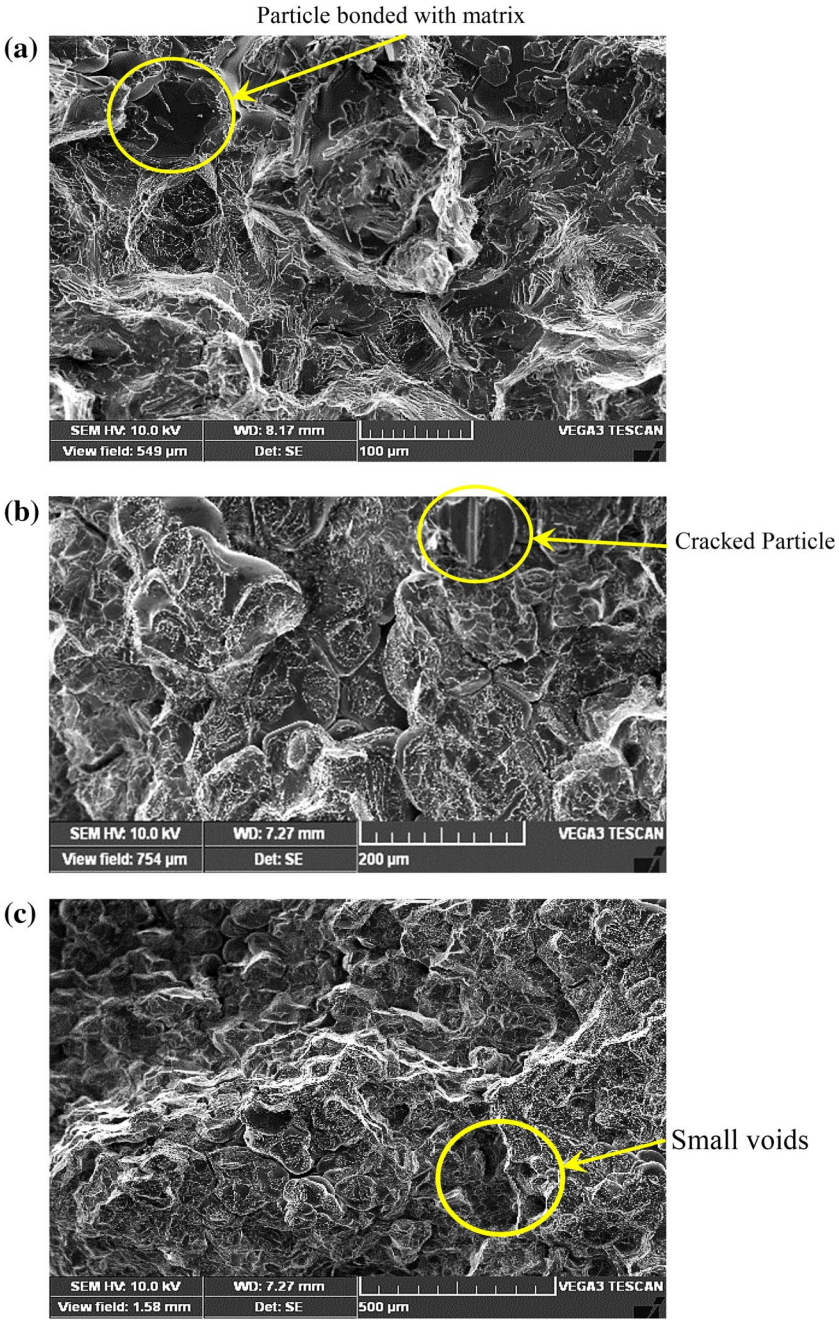

Fig. 10 FESEM micrographs of the fractured surface of joint formed with optimal parameter setting

gaps and discontinuities. However, while examining the joint obtained with initial setting of parameters using an optical microscope inbuilt with Clemex-Vision image analysing system, it was observed that the grains were pulled in the direction of rotation which can be attributed to the torque at elevated temperatures (Fig. 9a). However, the plastic zone was clearly evident and well defined in the microstructure of the joint obtained with the optimal parameters setting (Fig. 9b). Though the mechanism of heat generation was different from the fusion welding process, the temperature distribution from the weld zone to parent metal combined with the effect of torque had played an important role in creating different zones. Three regions were apparent in the interface of friction welded joints, namely the plastic zone (PZ), partially deformed zone (PDZ) around the bond line and the unaffected zone (UZ). These zones can be clearly visualized from the microstructure of optimal joint (Fig. 9b) in the form of the darker plastic region (plastic zone) compared to the unaffected zone [27, 29].

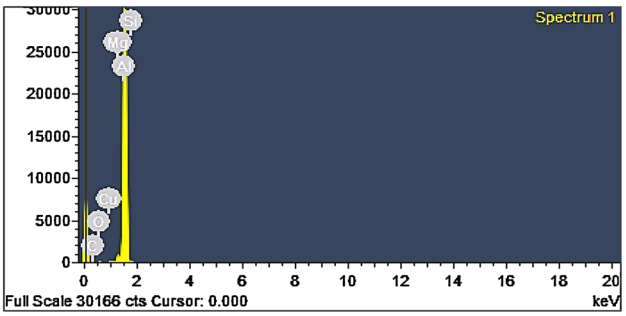

Fig. 11 EDX spectrum at the fractured surface

4.5 Characteristics of the fractured surface

After subjecting the optimal joint to tension test, the fractured surface was taken for analysis to study the mode of failure. The field emission scanning electron microscope (FESEM) images of the fractured surface of the joint are shown in Fig. 10. The presence of smaller voids and the coalescence of the matrix adjacent to these voids was evident (Fig. 10c). The reinforcement particles were dislodged due to external loading, forming the voids. The voids were of smaller size than the reinforcement indicating the ductile flow of matrix tending to cover up the empty spaces. Though the adhesion of reinforcement particles to the matrix was generally observed to be good (Fig. 10a), the particles on the verge of getting pulled from the matrix because of external loading become stress concentrators leading to voids. The optimal parameter setting had ensured sufficient generation of continuous frictional heat flux during the process of welding which was absolutely essential for plasticizing the material at the weld interface to produce high-quality joints. The failure mode of these aluminium-based composites were characterized by the coalescence of voids in the matrix, interfacial de-bonding at the particle–matrix interface and cracking of reinforcing particles [27]. These are clearly seen from the FESEM images shown in Fig. 10. A cracked particle partially covered by the plastically deformed matrix is also observed (Fig. 10b). This cracked particle partially covered by the surrounding matrix indirectly indicates the degree of good adhesion. These characteristics of the fractured surface indicate a ductile mode of failure. The energy-dispersive X-ray spectroscopy (EDX) analysis was also carried out on the fractured surface and is presented in Fig. 11. The profile obtained from elemental analysis shows the presence of silicon and carbon in the fractured surface available from the silicon carbide particles (reinforcement) and oxygen from the alumina particles (reinforcement).

5 Conclusion and future research

The paper presents an informative report on producing friction welded joints with Al/SiC/Al_2O_3 composite. The investigation had proved the effectiveness of friction welding in solid-state joining of MMCs. The following conclusions were drawn:

1. The microstructure of optimal joint had revealed the presence of three zones viz. plastic zone (PZ), partially deformed zone (PDZ) and unaffected zone (UZ), which coincides with the earlier findings.
2. An increased hardness was observed in the weld zone relative to the HAZ which was due to severe plastic deformation and localized strain hardening.
3. The presence of particle cracking and pull out (voids) were observed in the FESEM images of fractured surface and these were indicators of the ductile mode of failure of these joints.
4. Experimental welding optimization was performed using an integrated method of GT-PCA which combines the non-parametric approach of PCA with the uncertainty handling capabilities of grey theory. The optimal setting of parameters was predicted and confirmed as frictional pressure 60 MPa, upset pressure 120 MPa, burn off length 1 mm and rotational speed 2,250 rpm.
5. ANOVA was performed to supplement the GT-PCA approach. Frictional pressure was identified as the significant parameter to affect the responses with a contribution of 59.98 %, followed by the rotational speed with a contribution of 20.36 %.
6. The optimal combination of parameters predicted by the GT-PCA approach had significantly improved the S/N ratio and enhanced the quality characteristics (responses) studied in the process permitting the usage of GT-PCA technique for experimental welding optimization.
7. The joint formed with optimal setting of weld parameters showed symmetric flash, good matrix-reinforcement bonding and minimal voids in fractured surface with improved mechanical properties.

The research findings will offer the required guidelines and database for welding Al/SiC/Al_2O_3 composites using continuous drive friction welding process. The future scope lies in studying the effect of individual reinforcements on the properties of the joints which could be another contribution to the subject.

Acknowledgments The authors are grateful to IIT Madras for extending the facilities of metal joining laboratory to carry out the investigation. Further constant support from Mr M. Santhanakumar,

Department of Mechanical Engineering, Saveetha Engineering College, is highly appreciated.

References

1. Torralba JM, Da Costa CE, Velasco F (2003) P/M aluminum matrix composites: an overview. J Mater Proc Technol. 133(1–2):203–206
2. Urena A, Escalera MD, Gil L (2000) Influence of interface reactions on fracture mechanisms in TIG arc-welded aluminium matrix composites. Compos Sci Technol. 60(4):613–622
3. Durmus H, Meric C (2009) Weldability of AL99—SiC composites by CO_2 laser welding. J Compos Mater 43(13):1435–1450
4. Ananthapadmanaban D, Seshagiri Rao V, Abraham N, Prasad Rao K (2009) A study of mechanical properties of friction welded mild steel to stainless steel joints. Mater Des 30(7):2642–2646
5. Taban E, Gould JE, Lippold JC (2010) Dissimilar friction welding of 6061-T6 aluminum and AISI 1018 steel: properties and microstructural characterization. Mater Des 31(5):2305–2311
6. Sahin M (2010) Joining of aluminium and copper materials by friction welding. Int J Adv Manuf Technol 49(5–6):527–534
7. Rafi HK, Janaki Ram GD, Phanikumar G, Prasad Rao K (2010) Microstructure and tensile properties of friction welded aluminum alloy AA7075-T6. Mater Des 31(5):2375–2380
8. Sathiya P, Aravindan S, Noorul Haq A (2006) Optimization for friction welding parameters with multiple performance characteristics. Int J Mech Mater Des 3(4):309–318
9. Sahin M (2009) Characterization of properties in plastically deformed austenitic-stainless steels joined by friction welding. Mater Des 30(1):135–144
10. Deya HC, Ashfaq M, Bhaduria AK, Prasad Rao K (2009) Joining of titanium to 304L stainless steel by friction welding. J Mater Proc Technol 209(18–19):5862–5870
11. Krishnaiah K, Shahabudeen P (2012) Applied design of experiments and Taguchi methods. PHI Learning Pvt Ltd., New Delhi
12. Gauri SK, Pal S (2009) Comparison of performances of five prospective approaches for the multi-response optimization. Int J Adv Manuf Technol 48(9):1205–1220
13. Pal S, Malviya SK, Pal SK, Samantaray AK (2009) Optimization of quality characteristics parameters in a pulsed metal inert gas welding process using grey-based Taguchi method. Int J Adv Manuf Technol 44(11–12):1250–1260
14. Kumar S, Kumar S (2014) Multi-response optimization of process parameters for friction stir welding of joining dissimilar Al alloys by gray relation analysis and Taguchi method. J Braz Soc Mech Sci Eng. doi:10.1007/s40430-014-0195-2
15. Ghodsiyeh D, Golshan A, Izman S (2014) Multi-objective process optimization of wire electrical discharge machining based on response surface methodology. J Braz Soc Mech Sci Eng. 36(2):301–313
16. Ramkumar R, Ragupathy A (2014) Optimization of cooling tower performance with different types of packings using Taguchi approach. J Braz Soc Mech Sci Eng. doi:10.1007/s40430-014-0216-1
17. Lal S, Kumar S, Khan ZA, Siddiquee AN (2014) Wire electrical discharge machining of AA7075/SiC/Al_2O_3 hybrid composite fabricated by inert gas-assisted electromagnetic stir-casting process. J Braz Soc Mech Sci Eng 36(2):335–346
18. Kumar Jatinder (2014) Investigations into the surface quality and micro-hardness in the ultrasonic machining of titanium (ASTM GRADE-1). J Braz Soc Mech Sci Eng. 36(4):807–823
19. Madić M, Radovanović M (2013) Application of RCGA-ANN approach for modeling kerf width and surface roughness in CO_2 laser cutting of mild steel. J Braz Soc Mech Sci Eng. 35(2):103–110
20. Madić M, Radovanović M, Manić M, Trajanović M (2014) Optimization of ANN models using different optimization methods for improving CO_2 laser cut quality characteristics. J Braz Soc Mech Sci Eng. 36(1):91–99
21. Datta S, Nandi G, Bandyopadhyay A, Pal PK (2009) Application of PCA-based hybrid Taguchi method for correlated multicriteria optimization of submerged arc weld: a case study. Int J Adv Manuf Technol 45(3–4):276–286
22. Adalarasan R, Santhanakumar M, Shanmuga sundaram A (2014) Optimization of weld characteristics of friction welded AA 6061-AA 6351 joints using grey-principal component analysis (G-PCA). J Mech Sci Technol 28(1):301–307
23. Siddiquee AN, Khan ZA, Mallick Z (2010) Grey relational analysis coupled with principal component analysis for optimisation design of the process parameters in in-feed centreless cylindrical grinding. Int J Adv Manuf Technol 46(9–12):983–992
24. Kumar A, Kumar V, Kumar J (2014) Semi-empirical model on MRR and overcut in WEDM process of pure titanium using multi-objective desirability approach. J Braz Soc Mech Sci Eng. doi:10.1007/s40430-014-0208-1
25. Prabhu S, Uma M, Vinayagam BK (2013) Adaptive neuro-fuzzy interference system modelling of carbon nanotube-based electrical discharge machining process. J Braz Soc Mech Sci Eng. 35(4):505–516
26. Stalin John MR, Vinayagam BK (2014) Optimization of nonlinear characteristics of ball burnishing process using Sugeno fuzzy neural system. J Braz Soc Mech Sci Eng 36(1):101–109
27. Rotundo F, Ceschini L, Morri A, Jun TS, Korsunsky AM (2010) Mechanical and microstructural characterization of 2124Al/25 vol.%SiCp joints obtained by linear friction welding (LFW). Compos Part A 41(9):1028–1037
28. Bozkurt Y, Uzun H, Salman S (2011) Microstructure and mechanical properties of friction stir welded particulate reinforced AA2124/SiC/25p–T4 composite. J Compos Mater 45(21):2237–2245
29. Sathiya P, Aravindan S, Noorul Haq A (2007) A effect of friction welding parameters on mechanical and metallurgical properties of ferritic stainless steel. Int J Adv Manuf Technol 31(11–12):1076–1082
30. Narender singh P, Raghukandan K, Pai BC (2004) Optimization by grey relational analysis of EDM parameters on machining Al-SiCp10 % composites. J Mater Proc Technol 155–156:1658–1661
31. Noorul Haq A, Marimuthu P, Jeyapaul R (2008) Multi response optimization of machining parameters of drilling Al/SiC metal matrix composite using grey relational analysis in the Taguchi method. Int J Adv Manuf Technol 37:250–255